The Astrophysical Journal, 987:15 (10pp), 2025 July 1 https://doi.org/10.3847/1538-4357/addd12

Energetic Neutral Atom Fluxes from the Voyager 1 and 2 Directions

Stephen A. Fuselier[1,2], Eric J. Zirnstein[3], Jacob Heerikhuisen[4], André Galli[5], John D. Richardson[6], Daniel B. Reisenfeld[7], Nathan A. Schwadron[8], Maher A. Dayeh[1,2], David J. McComas[3], Herbert O. Funsten[7], Justyna M. Sokół[1], Merav Opher[9], Marc Z. Kornbleuth[9], and Jonathan Gasser[1]
[1] Southwest Research Institute, San Antonio, TX 78228, USA
[2] Department of Physics and Astronomy, University of Texas at San Antonio, San Antonio, TX 78249, USA
[3] Department of Astrophysical Sciences, Princeton University, Princeton, NJ 08544, USA
[4] Department of Mathematics and Statistics, University of Waikato, Hamilton, New Zealand
[5] Space Research & Planetary Science, Physics Institute, University of Bern, Bern, Switzerland
[6] Massachusetts Institute of Technology, Cambridge, MA, USA
[7] Los Alamos National Laboratory, ISR Division, Los Alamos, NM 87545, USA
[8] University of New Hampshire, Space Science Center, Durham, NH 03824, USA
[9] Department of Astronomy, Boston University, Boston, MA, USA
Received 2025 April 22; revised 2025 May 21; accepted 2025 May 25; published 2025 June 24

Abstract

IBEX observes a globally distributed energetic neutral atom (ENA) flux from the heliosheath and very local interstellar medium (VLISM). Over a 14 yr period, Voyager 1 and Voyager 2 traversed the heliosheath from the termination shock to the heliopause. In situ observations from these spacecraft place important constraints on the parent ion populations of the ENAs from the heliosheath in two directions on the upwind side of the heliosphere, i.e., the direction of motion of the Sun in the local interstellar medium. In this study, an MHD model that is constrained by Voyager in situ observations is used to estimate the contribution from the heliosheath to the total ENA fluxes observed by IBEX. At energies greater than about 0.5 keV, the heliosheath provides a significant fraction of the observed ENA flux. However, at energies less than about 0.5 keV, the heliosheath provides an insignificant fraction of the observed ENA flux. These results are the same for both directions, and since the Voyager 1 and 2 directions are not particularly unique, the results are likely to be applicable for much of the upwind hemisphere. Fundamentally, it is the physics of the termination shock and the thickness of the heliosheath that determine the energy-dependent contributions to the observed ENA flux from this region. Because the heliosheath source is insignificant, most ENAs at energies less than about 0.5 keV probably come from the VLISM.

Unified Astronomy Thesaurus concepts: Heliosphere (711); Heliopause (707); Heliosheath (710); Pickup ions (1239); Interstellar medium (847); Fast solar wind (1872); Solar wind (1534); Solar wind termination (1535)

1. Introduction to ENA Fluxes from the Heliosphere, Heliosheath, and VLISM

The interaction of the heliosphere with the local interstellar medium results in vast regions of space separated by relatively thin boundaries (see Figure 1). The heliosphere is the region that extends from the Sun to the heliopause. Inside of that, the supersonic solar wind expands out to the termination shock (at ~100 au, from the Sun). The heliosheath is the region beyond the termination shock and inside the heliopause (at ~150 au on the "upwind" side). Finally, the region beyond the heliopause where the heliosphere still has influence is the very local interstellar medium (VLISM; T. E. Holzer 1989), and this region extends many hundreds of au beyond the heliopause. Figure 1 shows these regions and boundaries in the upwind direction, that is, the direction of motion of the Sun relative to the local interstellar plasma and neutral gas. The focus of this investigation is on the boundaries and the plasma and neutrals in the upwind side of the heliosphere.

The heliosphere and heliosheath plasma contain several ion populations with different origins. In the heliosphere, the dominant ion population, by density, is the supersonic solar wind propagating radially away from the Sun. A second ion population is the pickup-ion population. Pickup ions are created by charge exchange of interstellar neutrals that entered the heliosphere. Upon charge exchange, newborn ions are picked up by the ExB force in the solar wind and rapidly form a shell velocity distribution centered on the solar wind bulk flow with radius equal to the solar wind velocity.

The solar wind is slowed, heated, and deflected across the termination shock. It continues to slow and deflect from the direction radially away from the Sun as it propagates through the heliosheath. Since the pickup-ion population has most of the energy upstream of the termination shock in the outer heliosphere, this population dominates the dissipation at the shock and is heated and slowed as it crosses the boundary into the heliosheath. Although the pickup-ion population has not been observed directly at the termination shock and immediately downstream in the heliosheath, Voyager 2 observations show that the core solar wind is not slowed and heated as much as would be expected if it dominated the dissipation at the shock (J. D. Richardson et al. 2008). These observations are indirect confirmation that pickup ions dominate this shock. Other observations of the importance of pickup ions in the heliosphere upstream of the termination shock include measurements of the pickup-ion density from 22 to 60 au from the Sun and an extrapolation of these densities to the termination shock at ~90 au (D. J. McComas et al. 2021; 2025). The SWAP instrument on the New Horizons spacecraft (D. J. McComas et al. 2008) measured a pickup-ion

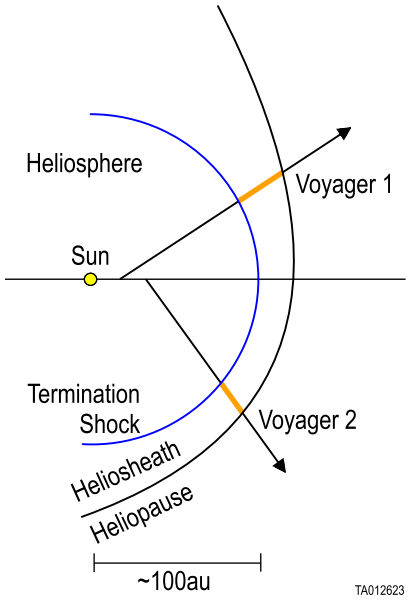

Figure 1. Side-view schematic of the boundaries and regions of the heliosphere in the upwind direction. The directions of the Voyager 1 and 2 spacecraft are shown, and the trajectories of these two spacecraft through the heliosheath from the termination shock to the heliopause are shown in orange. The distances to the termination shock and heliopause are approximately the same as those determined from IBEX observations of the changes in the ENA fluxes over more than a solar cycle.

density of about 12% of the solar wind density at 47 au and about 18% of the density at 60 au. This pickup-ion density is projected to increase to about 25%–30% of the solar wind density just upstream of the termination shock. By ∼20 au, the pickup-ion population already dominates the solar wind plasma and interplanetary magnetic field pressures, and this dominance only grows as the solar wind approaches the termination shock. Furthermore, SWAP observed preferential heating of pickup ions at interplanetary shocks in the outer heliosphere (E. J. Zirnstein et al. 2018; D. J. McComas et al. 2022; P. Mostafavi et al. 2025). This preferential heating at interplanetary shocks is indirect evidence that pickup ions are also preferentially heated at the termination shock.

The charge exchange process that produces pickup ions does not stop at the termination shock. Rather, it continues through the heliosheath, producing a second, "injected" pickup-ion population. This population's velocity distribution is centered on the core solar wind with shell radius equal to the slowed solar wind speed (E. J. Zirnstein et al. 2014; J. Heerikhuisen et al. 2019). There are other ion populations in the heliosphere, heliosheath, and VLISM (see, e.g., J. Heerikhuisen et al. 2010); however, the core solar wind and the two pickup-ion populations are the ones that are relevant for this investigation.

Ion populations in the heliosphere, heliosheath, and VLISM undergo charge exchange with interstellar neutrals that permeate all regions. They are the principal—or parent—ion populations of energetic neutral atoms (ENAs) that make up the diffuse, globally distributed hydrogen flux observed at 1 au by the ENA cameras on the IBEX spacecraft (H. O. Funsten et al. 2009b; D. J. McComas et al. 2009a; 2009b; S. A. Fuselier et al. 2021; A. Galli et al. 2023). This globally distributed flux of neutral hydrogen is observed at all energies measured by IBEX-Lo, from ∼0.01 to 2 keV (S. A. Fuselier et al. 2009), and IBEX-Hi, from ∼0.05 to 6 keV (H. O. Funsten et al. 2009a). The globally distributed flux is a probe of parent-ion populations and their interactions in the heliosphere, heliosheath, and beyond.

The fluxes and energies of the ENAs that are observed at 1 au depend strongly on the densities, radial velocities, and thermal speeds of the parent-ion populations in the heliosheath and on the line-of-sight path length from the termination shock to the heliopause.

To be observed as ENAs in the heliosphere at 1 au, parent ions that charge exchange must have a velocity component directed back into the heliosphere (in the Sun's frame of reference). That is, the velocity component must be in the direction opposite the radial direction away from the Sun. For example, in the heliosphere, the supersonic solar wind is much too cold (thermal energy ∼tens of eV) and moving too fast (bulk flow energy ∼1 keV) away from the Sun to have such a velocity component. However, some ions in the heated and slowed pickup-ion population in the heliosheath will have velocity components directed back into the heliosphere. From highest to lowest IBEX ENA energy, the parent-ion populations in the heliosheath that are the primary contributors to the globally distributed ENA flux are as follows (E. J. Zirnstein et al. 2014; J. Heerikhuisen et al. 2019; S. A. Fuselier et al. 2021):

(1) Accelerated pickup ions that produce ENAs with energies greater than a few keV. These are pickup ions that have been accelerated at the termination shock and in the heliosheath.
(2) Transmitted pickup ions that produce ENAs with energies ∼1 keV. These are pickup ions that dominate the termination shock structure.
(3) Injected pickup ions that produce ENAs with energies ∼hundreds of eV. These are pickup ions created in the heliosheath by charge exchange of the shocked solar wind in the region.
(4) Core solar wind ions that produce ENAs with energies ∼tens of eV. These are heated and slowed solar wind ions in the heliosheath.

The purpose of this paper is to investigate the relative contribution to the total ENA flux observed at 1 au from the heliosheath along two lines of sight, namely those of the Voyager 1 and 2 trajectories in the heliosheath. This paper is an extension of the investigation of ENA fluxes from the heliosheath that is presented in S. A. Fuselier et al. (2021) in two important ways. First, S. A. Fuselier et al. (2021) investigated contributions to the total ENA flux only in the Voyager 2 direction, finding that the contribution from the heliosheath was small, for ENA energies below ∼0.5 keV. This paper extends the investigation to include the Voyager 1 direction. Second, S. A. Fuselier et al. (2021) did not articulate why the heliosheath contribution to the ENA flux is small. Using a unique combination of modeling constrained by Voyager observations, this paper demonstrates why the contribution to the global ENA flux below ∼0.5 keV from the heliosheath is so small along both lines of sight and why it is likely small for the entire upwind hemisphere.

2. IBEX Observations

Figure 2 shows the ENA energy spectrum as measured by IBEX-Lo and -Hi from the lines of sight in the Voyager 1 and

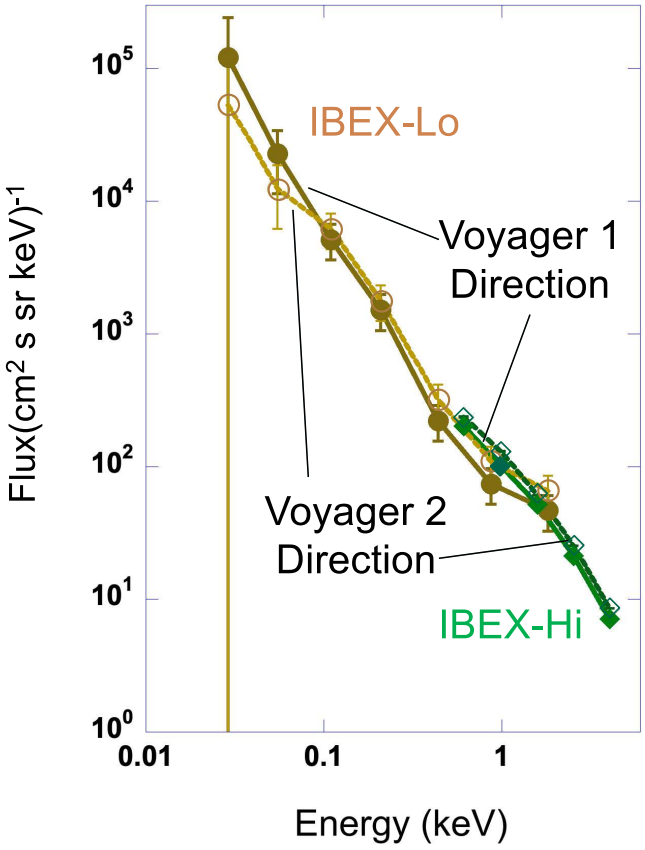

Figure 2. Energy spectra of ENAs from the Voyager 1 and Voyager 2 directions in the sky. The brown filled and open circles are ENA measurements from IBEX-Lo, and the green filled and open diamonds are ENA measurements from IBEX-Hi. The two energy spectra are very similar over the entire range of energies measured by IBEX.

2 directions. These fluxes were determined from the macro-pixels with 30° × 30° dimensions in the sky, centered approximately on the Voyager 1 and 2 directions. The fluxes from the Voyager 2 direction are the same as those used in S. A. Fuselier et al. (2021). The fluxes are from recent IBEX-Lo (A. Galli et al. 2022) and IBEX-Hi data releases (D. J. McComas et al. 2024). All IBEX-Hi fluxes are Compton–Getting corrected for the motion of the Earth and the spacecraft around the Sun, and include the latest survivability correction for ENA propagation from the heliosheath to 1 au. The IBEX-Hi energies reported below are for ENAs in the Sun-centered frame and are slightly different from the center energies of the instrument.

IBEX-Lo and -Hi were intercalibrated in the lab and on orbit; therefore, fluxes in Figure 2 from a particular direction match each other in the sensors' overlap energy range from 0.7 to 1.2 keV. Furthermore, this intercalibration and the periodic on-orbit detector tests account for any degradation in the signal over the 15 yr of IBEX-Lo and -Hi operations. The fluxes over the entire energy range are very similar in the two directions and are well represented by two power-law distributions with a knee at approximately 1 keV. In the remainder of the paper, an MHD model (see Section 4 for details), constrained by in situ observations from Voyager, is used to compute the contribution from the heliosheath to the ENA fluxes observed by IBEX in Figure 2.

3. Voyager 1 and 2 In Situ Observations

From 2007 August to 2018 November, Voyager 2 traversed the heliosheath, making solar wind plasma measurements from the termination shock to the heliopause (J. D. Richardson et al. 2019). The Plasma Science Experiment has used a calibration mode that demonstrated that the change in sensitivity has been at most a few percent throughout the almost 50 yr of operation (J. Belcher 2025, personal communication). The spacecraft crossed the termination shock at a radial distance of 84 au from the Sun and crossed the heliopause at a radial distance of 119 au. The measurements across the termination shock and in the heliosheath showed that the core solar wind slowed and heated approximately adiabatically across the shock. As the spacecraft traversed the heliosheath, further slowing of the core solar wind was observed, but the radial velocity did not go to zero until just before the crossing of the heliopause in late 2018. The density of the core solar wind increased by roughly a factor of 2 across the termination shock. Then, after a period of lower solar wind density that lasted about 2 yr, the density slowly increased by approximately a factor of 2 through the heliosheath. The temperature of the core solar wind increased somewhat across the termination shock and then remained low and relatively constant through the heliosheath.

From 2004 December to 2012 August, Voyager 1 traversed the heliosheath. The spacecraft crossed the termination shock three years before Voyager 2 at a radial distance of 94 au from the Sun and crossed the heliopause six years before Voyager 2 at a radial distance of ∼122 au. The spacecraft did not have an operational solar wind plasma instrument; therefore, no direct solar wind measurements were made along the trajectory. However, evidence from other instruments on the spacecraft and additional evidence from cross-analysis with Voyager 2 observations indicates that plasma parameters in the heliosheath along the Voyager 1 trajectory were likely similar to those observed by Voyager 2 along its trajectory. In particular, W. S. Kurth & D. A. Gurnett (2020) showed that plasma densities derived from the Voyager 1 plasma wave observations at and just downstream of the Voyager 1 termination shock were similar to the densities observed by the Voyager 2 plasma instrument at the Voyager 2 termination shock.

S. M. Krimigis et al. (2011) applied the Compton–Getting effect to observations from the low-energy charged particle (LECP) instrument to derive radial velocities along the Voyager 1 trajectory. They reported derived radial velocities that were approximately a factor of 2 lower than those observed by the Voyager 2 plasma instrument along its trajectory. Further, they reported that the derived radial velocity decreased to zero approximately 8 au before Voyager 1 crossed the heliopause. However, J. D. Richardson et al. (2021) argue that the radial velocities along the Voyager 1 trajectory were likely much more similar to those along the Voyager 2 trajectory. Further, they demonstrated that there were intervals along the Voyager 2 trajectory where the derived velocities from the LECP instrument on Voyager 2 were much lower than the measured velocities from the plasma instrument. Thus, it was unlikely that the radial velocity decreased to zero 8 au from the heliopause along the Voyager 1 direction. This underestimate of the derived radial velocities from the LECP instrument is supported by A. C. Cummings et al. (2021). These later authors also applied the Compton–

Getting effect to observations from the Cosmic Ray Subsystem to show that their derived radial velocities agreed with the observed velocities from the Voyager 2 plasma instrument. These indirect observations and direct comparisons between derived and measured densities and velocities suggest that Voyager 2 plasma observations could be used as a proxy for plasma conditions along the Voyager 1 direction. Therefore, in Section 5, the Voyager 2 plasma observations are used as constraints to derive heliosheath ENA fluxes from both the Voyager 1 and 2 directions.

4. Global Magnetohydrodynamic (MHD) Model for the Plasma along the Voyager 1 and 2 Trajectories

A global 3D MHD model coupled with a Monte Carlo particle code (J. Heerikhuisen et al. 2019) is used to simulate the plasma parameters in the heliosheath along the Voyager 1 and 2 directions. The MHD code uses a spherical grid with an inner boundary at 10 au and an outer boundary at 2500 au. The solar wind boundary conditions are determined by adiabatically expanding the following 1 au conditions to 10 au: 4.02 cm^{-3} density, 538 km s^{-1} velocity, 51,100 K temperature, and 3.75 nT radial component of the magnetic field. At the outer boundary, the conditions in the VLISM are as follows: 0.09 cm^{-3} proton density, 0.154 cm^{-3} neutral hydrogen density, 25.4 km s^{-1} flow speed of both components (relative to the Sun), and 7500 K neutral hydrogen temperature. To avoid the presence of an artificial flat current sheet while maintaining the presence of a magnetic field in the heliosphere, a unipolar field for the solar wind is adopted with magnetic field pointing away from the Sun in both the northern and southern hemispheres. More detail of the global heliosphere model is found in J. Heerikhuisen et al. (2019).

In S. A. Fuselier et al. (2021), the boundary conditions for the model run identified as "case IV" in J. Heerikhuisen et al. (2019) were used to model the plasma parameters along the Voyager 2 trajectory. An important result from the model run was that the shocked solar wind density was a factor of 2 higher than that observed by the plasma instrument along most of the Voyager 2 trajectory in the heliosheath. The modeled location of the termination shock differed significantly from the location observed by Voyager 2. However, the modeled and observed heliopause locations were in better agreement.

Two of the inner boundary conditions are different in the model run used here when compared to the inner boundary conditions used in S. A. Fuselier et al. (2021). The solar wind density at the inner boundary of the simulation is reduced by 30% (from 5.74 to 4.02 cm^{-3}) relative to the density in S. A. Fuselier et al. (2021). To keep the solar wind dynamic pressure approximately constant, the solar wind speed at the inner boundary is increased by the square root of 0.7 (from 450 to 636 km s^{-1}). Otherwise, the other boundary conditions, including the boundary conditions in the VLISM, are listed above and are the same as those in S. A. Fuselier et al. (2021), and by extension, case IV of J. Heerikhuisen et al. (2019).

Figure 3, panel (a), compares the density profile in the heliosheath from the model (dashed line) with the measured plasma density (solid line with error bars) along the Voyager 1 trajectory. In this panel, the Voyager 2 plasma density profile is used as a proxy for the Voyager 1 plasma measurements, and the time axis is that for the Voyager 2 traversal of the heliosheath, scaled to the heliosheath thickness along the Voyager 1 trajectory from the model. Panel (b) shows the three components of the solar wind bulk velocity in radial–tangential–normal (RTN) coordinates, where R is the Sun-Spacecraft unit vector, T is parallel to the Sun's spin direction, and N completes the right-handed system. The dashed lines are the three components from the model, and the solid lines with error bars are the measured solar wind velocity components along the Voyager 1 trajectory. In this panel, the Voyager 2 plasma velocity measurements are used as a proxy for the Voyager 1 velocities, except that the signs of the VT and VN components are reversed. The signs are reversed because Voyager 1 traversed the heliosheath north of the ecliptic and slightly starboard of the nose, i.e., the apparent direction of motion of the Sun in the interstellar medium, while Voyager 2 traversed the region south of the ecliptic and port of the nose. These 3D aspects of the Voyager 1 and 2 trajectories are not shown in the simplified 2D schematic in Figure 1. For these 3D aspects, see, e.g., D. J. McComas et al. (2009b) and S. A. Fuselier et al. (2021).

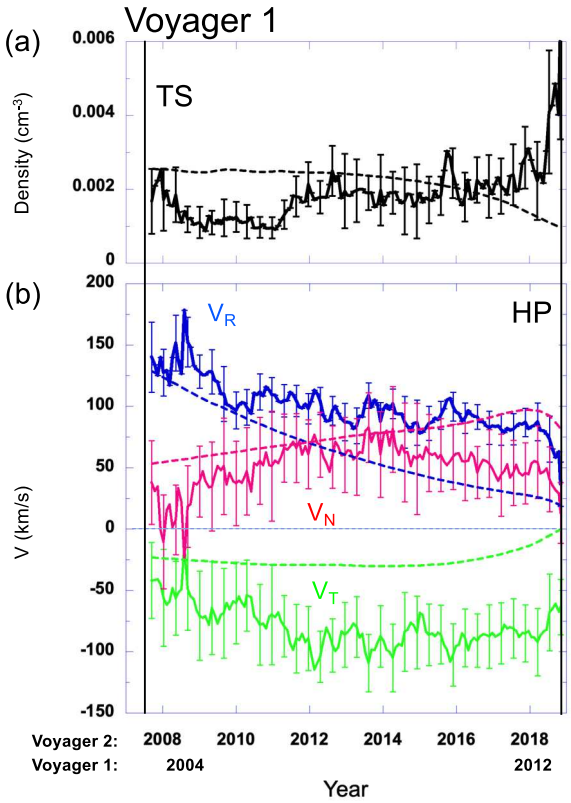

Figure 3. (a) The modeled solar wind ion density from the termination shock to the heliopause along the Voyager 1 direction (dashed line) compared to the solar wind density observed by Voyager 2 along its trajectory through the heliosheath (solid line). The modeled and observed densities agree reasonably well through the heliosheath, except for the first ~2–3 yr of the traversal and near the heliopause. (b) The modeled three components of the bulk flow velocity in the heliosheath in RTN coordinates (dashed lines) compared to the three velocity components observed by Voyager 2 along its trajectory. The Voyager 2 VT and VN component signs are reversed because Voyager 1 crossed the heliosheath at a different location relative to the nose than Voyager 2. The model underestimates the VT component, and more importantly, the VR component.

In Figure 4, panels (a) and (b) compare the modeled density and velocity component profiles in the heliosheath, respectively, from the model with those profiles measured along the Voyager 2 trajectory. The format is the same as in Figure 3. The Voyager 2 observations in Figure 4(b) are the same as those in S. A. Fuselier et al. (2021). However, the model

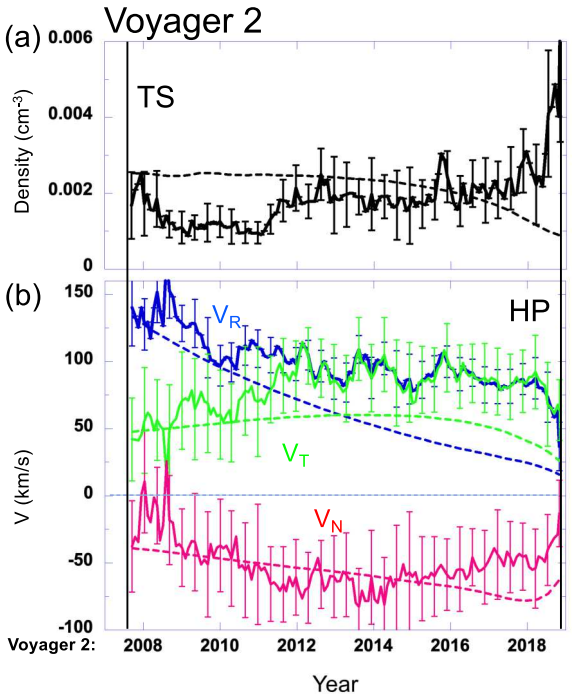

Figure 4. (a) The modeled solar wind ion density from the termination shock to the heliopause along the Voyager 2 direction (dashed line) compared to the solar wind density observed by Voyager 2 along its trajectory through the heliosheath (solid line). The modeled and observed densities agree reasonably well through the heliosheath except for the first ~2–3 yr of the traversal and near the heliopause. (b) The modeled three components of the bulk flow velocity in the heliosheath in RTN coordinates (dashed lines) compared to the three velocity components observed by Voyager 2 along its trajectory. Similarly to the results in the Voyager 1 direction, the model underestimates the VT component, and more importantly, the VR component in the Voyager 2 direction.

results are different because of the changes to the two inner boundary conditions. The modeled and observed densities are in better agreement except for the period just after the termination shock from 2008 to 2011 and the last part of the heliosheath before the heliopause starting around 2018. The modeled and observed VT and VN velocities are somewhat in agreement, but the modeled radial velocity is significantly lower than the observed velocity. The differences between the modeled and observed velocity components are larger in S. A. Fuselier et al. (2021); however, both model runs underestimate the radial velocity significantly.

Since the Voyager 2 plasma observations are used in the comparison between modeled and observed densities and velocities in Figure 3, the same agreements and disagreements between the modeled and observed parameters in Figure 4 persist in Figure 3. However, ignoring the observations in Figures 3 and 4 and comparing modeled densities and velocities in Figures 3 and 4, it is evident that, at least from a modeling-only perspective, the plasma environments in the two directions are similar.

Table 1 shows the comparisons among the observed and modeled termination shock and heliopause locations and heliosheath thicknesses. The model predicts a termination shock that is much closer to the Sun than the shock observed by either Voyager 1 or Voyager 2. It also predicts a somewhat thicker heliosheath than observed. The predicted and observed locations of the heliopause are not too dissimilar in the two directions. The predicted location of the termination shock in

Table 1
Observed and Modeled Locations of the Termination Shock and Heliopause and the Thicknesses of the Heliosheath

	Parameter	Modeled (au)	Observed (au)
Voyager 1	termination shock	74	94
	heliopause	116	122
	heliosheath thickness	42	28
Voyager 2	termination shock	75	84
	heliopause	116	119
	heliosheath thickness	41	35

the Voyager 2 direction in Table 1 is similar to the predicted location in S. A. Fuselier et al. (2021). This similarity is a direct result of the effort to keep the modeled solar wind dynamic pressure at the inner boundary nearly the same in the two simulations. The differences in the modeled and observed heliosheath thicknesses in Table 1 highlight the motion of the boundaries of the heliosheath over the Voyager 1 and 2 traversals of the region. The model does not have any time dependence, and therefore, the thickness of the heliosheath in the Voyager 1 and 2 directions is nearly the same. However, it took about 11 yr for Voyager 2 to traverse the heliosheath and only about 8 yr for Voyager 1 to traverse the region. While Voyager 2 is traveling about 10% slower than Voyager 1, the speed differential cannot account for the differences in the perceived thicknesses of the heliosheath.

The higher solar wind speed used here compared to that used in S. A. Fuselier et al. (2021) results in higher thermal velocities for the pickup-ion populations in the heliosphere, and consequently, an increase in the termination shock strength. In general, it is difficult to make a detailed comparison of modeled and observed parameters because the model run uses steady-state plasma boundary conditions while the Voyager spacecraft crossed boundaries 4–6 yr apart and spent more than a decade in the heliosheath. During such a long span of time, solar wind conditions change dramatically. Such a comparison is not necessary for the purposes of this paper, because model results and observations are normalized to the boundary locations and heliosheath thickness observed by Voyager 2. For more detail on time-dependent models, see, e.g., E. J. Zirnstein et al. (2022).

5. ENA Fluxes from the Heliosheath in the Voyager 1 and 2 Directions

The ENA flux from the heliosheath in the Voyager 1 and Voyager 2 directions is determined from Equation (1) (taken from S. A. Fuselier et al. 2021). $J_{\rm ENA}(E)$ is the energy-dependent ENA flux, and the integral is along the line of sight from the termination shock to the heliopause. The interstellar neutral hydrogen density, $n_{\rm H}(R)$, is a function of radial distance, but here, as in S. A. Fuselier et al. (2021), this density is assumed to be equal to $0.127 \pm 0.015\,{\rm cm}^{-3}$ (P. Swaczyna et al. 2020) and constant throughout the heliosheath. Energy-dependent cross sections, $\sigma(E)$, are from B. G. Lindsay & R. F. Stebbings (2005) and are the same as used in S. A. Fuselier et al. (2021). Finally, $J_{\rm Ion}(E,R)$, the energy- and radial-distance-dependent ion flux, is determined from the MHD model with constraints applied from the Voyager observations in Figures 3 and 4. That is, densities of the pickup-ion distributions are normalized by the ratio of the

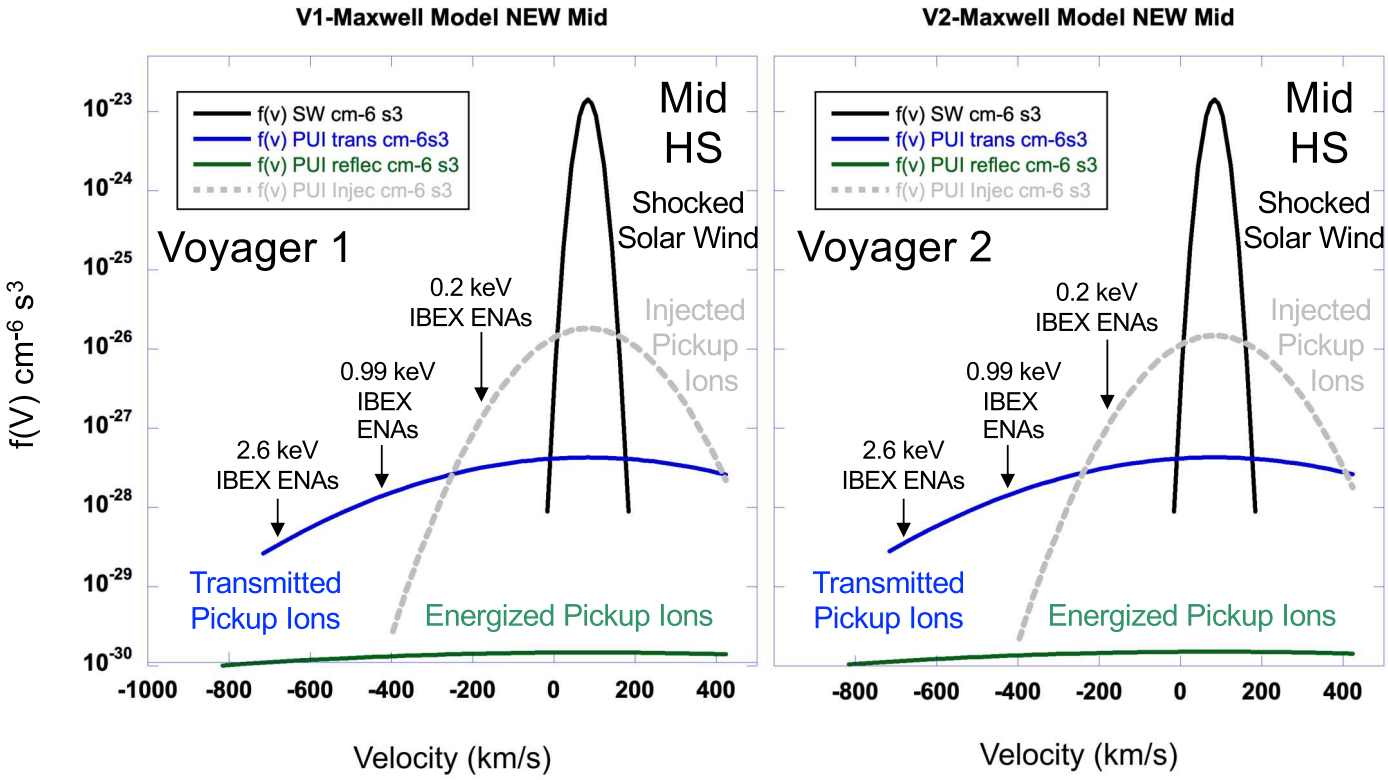

Figure 5. One-dimensional cuts in the shocked solar wind and pickup-ion populations for the Maxwellian model at the midpoint in the heliosheath. The cuts are along the radial direction, and the frame of reference is the Sun. Ions with negative velocities that charge exchange with interstellar neutrals will produce ENAs that are detectable by IBEX. Three of the IBEX ENA energies are shown. For energies above about 0.5 keV, the parent-ion population that contributes most to the ENA flux is the transmitted pickup-ion population. For energies below 0.5 keV, the injected pickup-ion population contributes most to the ENA flux. The core solar wind is too cold and moving too fast away from the Sun to contribute to ENA fluxes in the IBEX energy range.

observed to modeled solar wind density, and the radial components of the bulk velocities of the pickup-ion distributions are set to the observed solar wind bulk velocities:

$$J_{\rm ENA}(E) = \int dR\, n_{\rm H}(R) J_{\rm Ion}(E, R)\sigma(E). \quad (1)$$

Equation (1) is solved by converting the integral into a sum over distance elements in the heliosheath that have $dR = \Delta R \sim 0.5$ au, which corresponds to about 60 day averages of the Voyager 2 plasma observations (see Equation (2)). In S. A. Fuselier et al. (2021), two pickup-ion models were used to characterize the pickup-ion populations: a Maxwellian model and a shell model. These were used to quantify the possible range of ENA fluxes that result from a particular pickup-ion model. Here, only the Maxwellian model is used to describe the core solar wind, as well as the injected, transmitted, and energized pickup-ion populations (E. J. Zirnstein et al. 2014; J. Heerikhuisen et al. 2019; B. L. Shrestha et al. 2020). It describes each population as a Maxwell–Boltzmann distribution and all populations comove with the core solar wind. The Maxwellian assumption implies that there is nearly instantaneous energy diffusion for individual pickup-ion populations, but there is insufficient energy diffusion to create a single Maxwellian centered on the core solar wind.

As in S. A. Fuselier et al. (2021), the core, shocked solar wind, and pickup-ion populations at three locations in the heliosheath from the MHD model are used to interpolate the ion fluxes at all other locations in the region. At these three locations, the densities of all ion populations are normalized by the ratio of the shocked solar wind density measured by Voyager to the modeled solar wind density. Similarly, the bulk velocities of all ion populations are normalized to the shocked solar wind velocity measured by Voyager 2. Figure 5 shows the phase space densities of the pickup-ion populations and the core solar wind at the midpoint in the heliosheath in the Voyager 1 and 2 directions. This figure is similar to Figure 3 in S. A. Fuselier et al. (2021). The one-dimensional cuts in the distributions in Figure 5 are along the radial direction, and the frame of reference is the Sun. The shocked solar wind, as measured by Voyager 2, is moving away from the Sun with a radial velocity of 84 km s^{-1}, and all pickup-ion populations are centered on this radial velocity.

Also shown in Figure 5 are the energies of ENAs produced by charge exchange of pickup ions that have the appropriate velocity directed back into the heliosphere, i.e., at negative velocities. These are ENAs that are detected by IBEX at 1 au. Two IBEX-Hi energies at 2.6 keV and 0.99 keV and one IBEX-Lo energy at 0.2 keV are shown. ENAs with energies between about 0.5 and 2.6 keV are predominantly from charge exchange of transmitted pickup ions that have dominated the termination shock process. ENAs with energies less than about 0.5 keV are predominantly from charge exchange of injected pickup ions. Thus, the lower energies of IBEX-Lo probe the injected ion population, and IBEX-Hi probes the transmitted pickup-ion population. The flux of shocked solar wind ions with negative velocities is extremely low; therefore, IBEX does not detect any ENAs from this population at this location in the heliosheath. The energized pickup ions that are accelerated at the termination shock and in the heliosheath

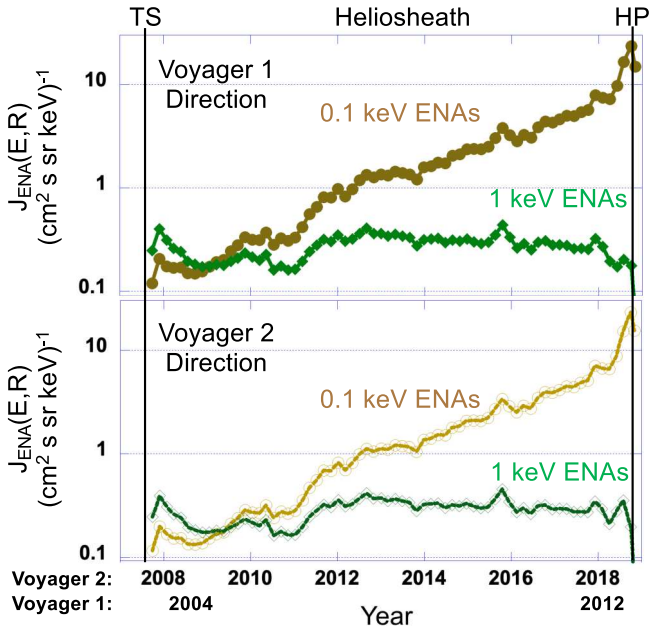

Figure 6. ENA flux produced at each point in the heliosheath along the Voyager 1 and 2 directions for two different energies. Summing the fluxes at each point produces the total flux along the Voyager 1 and 2 lines of sight in the sky. ENAs at 1 keV are in the IBEX-Hi energy range and are from charge exchange of the transmitted pickup-ion population. This parent-ion population is heated at the termination shock and changes very little through the heliosheath. Thus, its contribution to the ENA flux is relatively constant and simply reflects the variations in the pickup-ion density, which comprise a nearly constant fraction of the core solar wind. ENAs at 0.1 keV are in the IBEX-Lo energy range and are primarily from charge exchange of the injected pickup-ion population. This parent-ion population is produced continuously through the heliosheath. As a result, its contribution increases exponentially through the heliosheath, with the largest contribution coming from approximately the last third of the trajectory.

also have very low fluxes and probably do not contribute to the ENA flux, even at the two highest IBEX-Hi energies of 2.7 keV and 4.3 keV (average values).

Figure 6 shows the ENA flux (from Equation (2)) at points along the Voyager 1 and 2 trajectories for two ENA energies. In Equation (2), ΔR is the distance segment in the heliosheath along the Voyager 1 or 2 trajectory and is ~0.5 au. The total ENA flux along the line of sight is the sum over all $J_{\rm ENA}(E,R)$ in Figure 6 from the termination shock to the heliopause:

$$J_{\rm ENA}(E,\,R) = \Lambda R\, n_H(R) J_{\rm Ion}(E,\,R)\sigma(E). \quad (2)$$

The ENA flux profiles at the two energies are different through the heliosheath. For 1 keV ENAs, Figure 6 shows that the contribution to the total ENA flux from the heliosheath is nearly constant. The decrease just after the termination shock and the subsequent increase after year 3 reflect the observed solar wind density profile in Figures 3 and 4, since all pickup-ion fluxes are normalized by this observed solar wind density profile. Otherwise, the nearly constant ENA profile reflects the fact that transmitted pickup ions at these energies are accelerated at the termination shock, and after this initial acceleration, there is relatively little change in their energy or density through the heliosheath.

For 0.1 keV ENAs, the flux profile is very different. There is the same decrease and then increase near the beginning of the heliosheath interval that is associated with the solar wind density normalization. However, in the log plot in Figure 6, the flux increases linearly, such that ENAs produced in

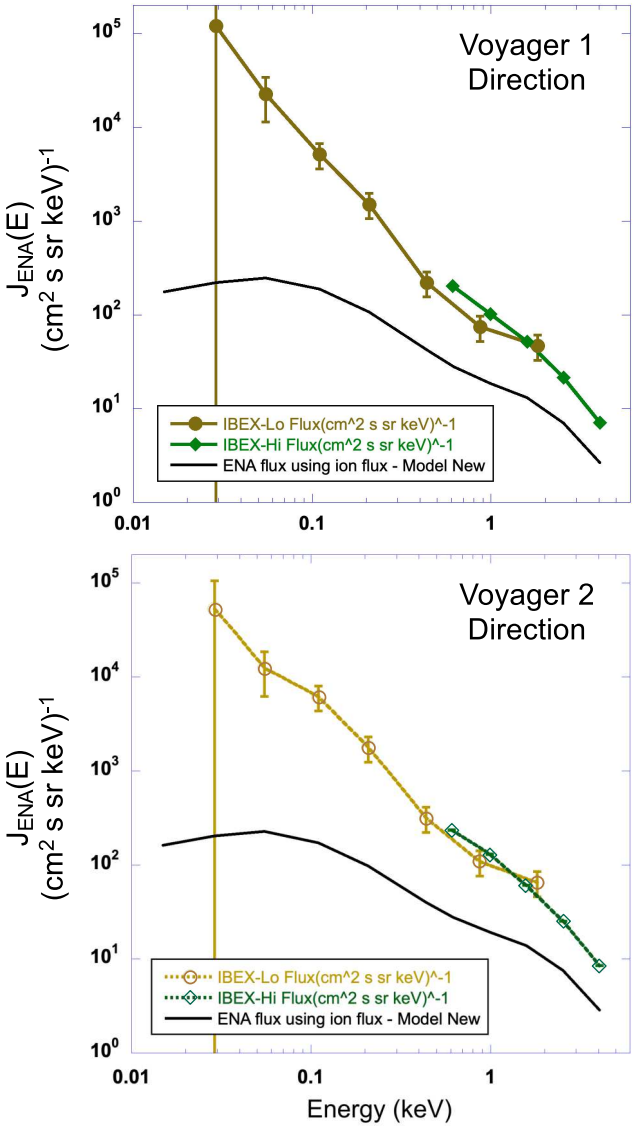

Figure 7. Comparison of the observed ENA flux from the Voyager 1 (a) and Voyager 2 (b) directions with the predicted contributions from the model constrained by the Voyager 2 in situ observations. In both directions and at energies greater than about 0.5 keV, the predicted fluxes from the heliosheath are between about 15% and 30% of the observed total fluxes. For energies less than 0.5 keV, the predicted fluxes from the heliosheath are an insignificant percentage (i.e., at most a few percent) of the observed total fluxes in both directions.

approximately the last one-third to one-quarter of the trajectory through the heliosheath dominate the total ENA flux. This steady increase reflects the steady increase in injected pickup ions, and to a lesser extent, the steady slowing of the shocked solar wind through the heliosheath (see Figures 3 and 4).

Figure 7 compares the observed ENA flux from the Voyager 1 (panel (a)) and Voyager 2 (panel (b)) directions with the predicted contributions from the heliosheath computed from Equations (1) and (2). The observed fluxes in both directions are very similar (Figure 1), and Figure 7 shows that the predicted fluxes from the heliosheath in both directions are also very similar. The model predicts a significant contribution to the total ENA flux at energies greater than 1 keV. However, for energies less than about 0.5 keV, the observed ENA flux continues to increase steeply. The predicted contribution from

Table 2
Comparison of Predicted and Observed ENA Fluxes at Three Energies from the Voyager 1 and Voyager 2 Directions

Direction	ENA Energy (keV)	Predicted % Contribution from Heliosheath to Total ENA Flux (%)	Predicted % Contribution from Heliosheath to Total ENA Flux—for Zero Radial Velocity in Final 8 au (%)
Voyager 1	0.11	4 ± 1[a]	2 ± 1
	0.99	18	18
	2.55	33	33
Direction	ENA Energy (keV)	Predicted % Contribution from Heliosheath to Total ENA Flux (%)	Predicted % Contribution from Heliosheath to Total ENA Flux—from S. A. Fuselier et al. (2021) (%)
Voyager 2	0.11	3 ± 1	3 ± 1
	0.99	15	10
	2.55	30	13

Note.
[a] The uncertainties on the predicted contributions for the two IBEX-Hi energies (0.99 and 2.55 keV) are much less than 1% and are therefore not listed.

the heliosheath increases much more slowly, and this predicted contribution eventually reaches a shallow maximum at about 0.05 keV. At 0.1 keV, the contribution is insignificant.

6. Discussion and Conclusions

An MHD model was used to determine the ion fluxes of the solar wind and pickup-ion populations in the heliosheath. This model was constrained by Voyager 2 observations of the shocked solar wind density and velocity that were made during its traversal of the heliosheath from the termination shock to the heliopause. The constraints from the Voyager 2 observations were also imposed on the trajectory of Voyager 1 through the heliosheath. The MHD model was similar to the one used in S. A. Fuselier et al. (2021) except that, at the inner boundary of the simulation, the solar wind density was reduced by a factor of 2, and the solar wind velocity was increased by a factor of the square root of 2. These solar wind conditions were the same for all radial directions, and there is no time variability in the simulation. The increase in the solar wind velocity at the inner boundary of the simulation results in an increase in the termination shock strength. This increased shock strength has consequences for the contributions of the transmitted pickup-ion population in the heliosheath to the total ENA flux observed by IBEX.

The modeled ion fluxes and in situ plasma observations were used to determine the ENA flux from the heliosheath in the Voyager 1 and Voyager 2 directions. In Figure 7, these fluxes were compared to the observed fluxes from IBEX. The modeled flux from the heliosheath accounts for between 15% and 30% of the total observed ENA flux for energies greater than 0.5 keV and at most a few percent of the total observed ENA flux for energies less than about 0.5 keV. Table 2 quantifies these percent contributions at three IBEX energies: 0.11, 0.99, and 2.55 keV.

For ENA energies greater than about 0.5 keV, the parent-ion population is the transmitted pickup population. For the Voyager 2 direction, Table 2 compares the fractional contributions from the heliosheath for 0.99 and 2.55 keV with contributions at those energies from S. A. Fuselier et al. (2021). In the simulation used here, the termination shock is stronger than that in S. A. Fuselier et al. (2021). As a direct consequence of this increase in shock strength, the contribution from the heliosheath increased by a factor of 1.5 at 0.99 keV and by more than a factor of 2 at 2.55 keV. This comparison illustrates the strong coupling between ENA production in the heliosheath and termination shock strength. The simulations used here and in S. A. Fuselier et al. (2021) used fixed boundary conditions. Other, time-dependent simulations (E. J. Zirnstein et al. 2022; J. Giacalone et al. 2025) used the time history of solar wind conditions observed at 1 au during the traversal of Voyager 2 through the heliosheath as inner boundary conditions. These simulations and others (e.g., M. Gkioulidou et al. 2022; M. Kornbleuth et al. 2023) emphasize the transmitted pickup-ion population's role in producing ENAs with energies greater than 0.5 keV. E. J. Zirnstein et al. (2022) and J. Giacalone et al. (2025) also show that variations in the termination shock strength during the Voyager 2 traversal of the heliosheath could account for most of the difference between the predicted ENA contribution from the heliosheath and the observed ENA fluxes for energies greater than about 0.5 keV. For example, E. J. Zirnstein et al. (2022) concluded that the heliosheath source accounts for greater than 80% of the observed total ENA flux for energies greater than about 0.5 keV.

There is other indirect evidence that the heliosheath is the dominant source of ENAs at energies greater than 0.5 keV. D. B. Reisenfeld et al. (2021) showed that changes in the globally distributed ENA flux observed at 1 au by IBEX were consistent with a source that was located less than about 110–120 au from the Sun in the nose direction and came from a heliosheath that was ∼30–45 au thick. This distance and thickness are reasonably consistent with the location of the heliopause and thickness of the heliosheath that were determined from the Voyager observations.

Summarizing the results for ENA energies greater than 0.5 keV, the assumed shape or form of the parent-ion population and time variability are critical for determining the heliosheath contribution to the ENA flux. The parent, transmitted pickup-ion population has been assumed to be a shell distribution (S. A. Fuselier et al. 2021), a kappa distribution (e.g., M. Gkioulidou et al. 2022; M. Kornbleuth et al. 2023), or a distribution that varies with time in response to variable solar wind condition upstream of the termination

shock changes (E. J. Zirnstein et al. 2022; J. Giacalone et al. 2025). All these assumed forms of the distribution yield consistent results that point to this heliosheath population as the dominant contributor to observed ENAs with energies greater than 0.5 keV.

In contrast to the results for energies greater than about 0.5 keV, Figure 7 and Table 2 show that the heliosheath contribution to the total ENA flux at energies less than about 0.5 keV is insignificant. These results have been reported previously by S. A. Fuselier et al. (2021) for the Voyager 2 direction and A. Galli et al. (2023) for several directions in the upwind hemisphere.

In Table 2, the predicted contributions from the heliosheath in the Voyager 2 direction for two different termination shock strengths are compared. In S. A. Fuselier et al. (2021), the termination shock strength was less than that in the simulation used here. While it is clear that the termination shock strength has a significant effect on the ENA flux from the heliosheath at 0.99 and 2.55 keV, it has essentially no effect on the ENA flux from the heliosheath at 0.11 keV. This difference occurs because the transmitted pickup ions are not the dominant parent-ion population for ENAs less than 0.5 keV (see Figure 5).

One potential source for ENAs from the heliosheath with energies less than 0.5 keV is the injected pickup ions (see Figure 5). These ions are created in the heliosheath, and their contribution to, e.g., 0.11 keV ENAs increases through the heliosheath, such that the majority of the ENAs come from the last one-third to one-quarter of the heliosheath before the heliopause (see Figure 6). However, the heliosheath in the upwind direction is not thick enough for the injected pickup-ion population to contribute significantly to the observed ENA flux at 0.11 keV.

The model predicts a thicker heliosheath than observed by either Voyager 1 or Voyager 2 (see Table 1). However, the differences are less than 10 au out of about 40 au thickness. In Figure 6, 0.11 keV ENA fluxes of $\sim$10 cm^2 s Sr keV are produced close to the heliopause. Extrapolating the increasing flux trend to larger radial distances, the heliosheath would have to be on the order of 2–3 times thicker, i.e., a thickness of 80–120 au, for the injected pickup-ion population to be the dominant parent-ion population for 0.11 keV ENAs in Figures 2 or 7. Such a thick heliosheath is inconsistent with the Voyager 2 observations of the heliosheath thickness in Table 1. An 80–120 au thick heliosheath is also inconsistent with the heliopause thickness and heliopause distance in the upwind hemisphere derived from variations in ENA fluxes at higher energies (D. B. Reisenfeld et al. 2021). Furthermore, an 80–120 au thick heliosheath would produce on the order of 2–3 times the ENA flux at energies greater than 0.5 keV. These very high fluxes are inconsistent with predicted ENA fluxes at these energies (E. J. Zirnstein et al. 2022).

The injected pickup-ion population could be modified by either substantial slowing of the radial velocity of the solar wind or by turbulence in the heliosheath. However, these modifications do not result in a substantial increase in ENA fluxes, especially at 0.11 keV. The reason for the lack of a substantial increase is that the slowing of the distribution or turbulence cannot increase the peak phase space density for the injected pickup ions. In Figure 5, the peak phase space density of the injected pickup-ion population is determined by its number density, and this number density is limited by the production of pickup ions in the relatively thin heliosheath.

Table 2 demonstrates that the bulk velocity of the injected population has little effect on its contribution to 0.11 keV ENAs. For Voyager 1, the contributions to 0.11 keV ENAs are shown for two different radial velocity profiles. The first is the observed radial velocity profile for Voyager 2, and the second is the same radial velocity profile except that the radial velocity is set to zero within 8 au of the heliopause. The substantial slowing of the radial velocity has little effect on the heliosheath contribution to the ENA fluxes at any of the three energies listed.

Recently, S. Du et al. (2025) suggested that, if the magnetic field in the heliosheath is exactly perpendicular to the radial line of sight and there were no pitch angle scattering of the newly created, injected pickup ions, then the phase space density of this population would be substantially larger than the isotropic distribution shown in Figure 5. S. Du et al. (2025) argue that the phase space density could increase by more than a factor of 100 with these assumptions. However, S. Du et al. (2025) also point out that the assumption that there is no pitch angle scattering probably only applies close to the termination shock, where the injected pickup-ion population has very low density. As seen in Figure 6, this region near the termination shock contributes the least to the total ENA flux at 0.1 keV. Closer to the heliopause, the plasma beta is expected to approach 1 (e.g., S. A. Fuselier et al. 2020), and plasmas with beta values near one do not allow ion temperature anisotropies greater than about a factor of 2 (e.g., S. P. Gary et al. 1994).

In addition, the variation of the observed magnetic field direction through the heliosheath along, e.g., the Voyager 1 trajectory, places very strong constraints on the anisotropy and the apparent variation of the phase space density with pitch angle as observed from the Sun. L. F. Burlaga & N. F. Ness (2012) show that the elevation angle of the magnetic field in the heliosheath, while centered on the direction perpendicular to the line of sight, varies by more than $\pm 45^\circ$ about this direction through the heliosheath. The pitch angle distribution of the injected pickup-ion population is the result of ion pickup all along the trajectory. Therefore, the injected pickup ions will be approximately uniformly spread over more than $\pm 45^\circ$ in pitch angle centered on 90°. This spread greatly reduces the anisotropy of the population without any additional scattering due to wave–particle interactions. Furthermore, there are significant intervals in the heliosheath when the ENAs produced along the line of sight will not come from ions at pitch angles of 90°. For these reasons, the anisotropy of the injected pickup-ion population is likely less than a factor of 2 along a substantial portion of the line of sight. Therefore, this anisotropic distribution likely results in less than a factor of 2 increase in the ENA flux at energies less than 0.5 keV above estimates assuming an isotropic ion distribution.

In summary, constraints from observations and modeling indicate that turbulence, significant bulk flow velocity changes, or temperature anisotropies are not able to produce a substantial increase in the contribution to the ENA flux from the injected pickup-ion population in the heliosheath.

Another potential source for ENAs at energies less than 0.5 keV is the core solar wind. The difficulty with this source is that the core solar wind does not appear to be slowed enough and heated enough to produce ENAs in the energy range of a few hundred eV (J. D. Richardson et al. 2008). One possibility is that the radial velocity of the core solar wind slows to zero within 8 au of the heliopause (S. M. Krimigis et al. 2011). As

discussed above, Table 2 contains the results of a test of this possibility along the Voyager 1 direction. There is no effect on the contributions to the ENA flux at 0.99 and 2.55 keV because the core solar wind is too cold to contribute to the ENA flux at these high energies. There is also little or no change in the contribution to the ENA flux at 0.11 keV either for the same reason. To contribute to the ENA flux at 0.11 keV, the core solar wind would have to heat by more than a factor of 10. This significant heating is inconsistent with Voyager 2 observations (J. D. Richardson et al. 2008), inconsistent with heating observed at interplanetary shocks in the outer heliosphere (E. J. Zirnstein et al. 2018; D. J. McComas et al. 2022; P. Mostafavi et al. 2025), and inconsistent with the theoretical understanding of a pickup-ion-mediated termination shock (e.g., E. J. Zirnstein et al. 2022; J. Giacalone et al. 2025). In short, the shock physics that dictates that the majority of the ENAs at energies greater than 0.5 keV come from the heliosheath is the same physics that dictates that the core solar wind cannot contribute to the ENA flux at IBEX-Lo energies between about 0.005 and 0.5 keV.

The Voyager 1 and 2 directions are not unique to the upwind hemisphere. Therefore, the results presented here are applicable to the globally distributed ENA fluxes coming from any direction in the upwind hemisphere. If the heliosheath is not the primary source of ENAs with energies less than 0.5 keV, then the only other potential primary source is the VLISM. One advantage of the VLISM source is that the integral path length in Equation (1) could be much longer than the heliosheath thickness. It remains to be seen if this region can be modeled to account for the ENA fluxes at energies less than 0.5 keV in Figures 1 and 7.

Acknowledgments

Support for this study comes from the IBEX mission as a part of NASA's Explorer program under grant 80NSSC20K0719 and IMAP mission as a part of NASA's Solar Terrestrial Probes (STP) Program (80GSFC19C0027). Several of the authors were supported under NASA grant 18-DRIVE18_2-0029, Our Heliospheric Shield, 80NSSC20K0603. IBEX is 15+ years into its 2 yr science mission and is not showing any signs of diminished science return. All who contributed to this mission share in its continued success. Similarly, all who contributed to the Voyager mission share in its continued success.

Data Availability

IBEX-Hi data in this paper are from data release 16 and are available at https://ibex.princeton.edu/DataRelease16. IBEX-Lo data in this paper are from data release 17 and are available at https://ibex.princeton.edu/DataRelease17. The Voyager data are available at https://omniweb.gsfc.nasa.gov/.

ORCID iDs

Stephen A. Fuselier https://orcid.org/0000-0003-4101-7901
Eric J. Zirnstein https://orcid.org/0000-0001-7240-0618
Jacob Heerikhuisen https://orcid.org/0000-0001-7867-3633
André Galli https://orcid.org/0000-0003-2425-3793
John D. Richardson https://orcid.org/0000-0003-4041-7540
Daniel B. Reisenfeld https://orcid.org/0000-0003-1874-9450
Nathan A. Schwadron https://orcid.org/0000-0002-3737-9283
Maher A. Dayeh https://orcid.org/0000-0001-9323-1200
David J. McComas https://orcid.org/0000-0001-6160-1158
Herbert O. Funsten https://orcid.org/0000-0002-6817-1039
Justyna M. Sokół https://orcid.org/0000-0002-4173-3601
Merav Opher https://orcid.org/0000-0002-8767-8273
Marc Z. Kornbleuth https://orcid.org/0000-0002-3479-1766
Jonathan Gasser https://orcid.org/0000-0002-9237-7088

References

Burlaga, L. F., & Ness, N. F. 2012, ApJ, 749, 13
Cummings, A. C., Stone, E. C., Richardson, J. D., et al. 2021, ApJ, 906, 126
Du, S., Opher, M., & Kornbleuth, M. 2025, ApJL, 982, L59
Funsten, H. O., Allegrini, F., Bochsler, P., et al. 2009a, SSRv, 146, 75
Funsten, H. O., Allegrini, F., Crew, G. B., et al. 2009b, Sci, 326, 964
Fuselier, S. A., Bochsler, P., Chornay, D., et al. 2009, SSRv, 146, 117
Fuselier, S. A., Galli, A., Richardson, J. D., Reisenfeld, D. B., et al. 2021, ApJL, 915, L26
Fuselier, S. A., Petrinec, S. M., Bobra, M. G., et al. 2020, JPhCS, 1620, 012004
Galli, A., Baliukin, I. I., Kornbleuth, M., Opher, M., et al. 2023, ApJL, 954, L24
Galli, A., Wurz, P., Schwadron, N. A., Fairfield, K., et al. 2022, ApJS, 261, 18
Gary, S. P., McKean, M. E., Winske, D., et al. 1994, JGR, 99, 5903
Giacalone, J., Kornbleuth, M., Opher, M., Gkioulidou, M., et al. 2025, ApJ, 980, 29
Gkioulidou, M., Opher, M., Kornbleuth, M., et al. 2022, ApJL, 931, L21
Heerikhuisen, J., Pogorelov, N. V., Zank, G. P., et al. 2010, ApJL, 708, L126
Heerikhuisen, J., Zirnstein, E. J., Pogorelov, N. V., et al. 2019, ApJ, 874, 76
Holzer, T. E. 1989, ARA&A, 27, 199
Kornbleuth, M., Opher, M., Zank, G. P., et al. 2023, ApJL, 944, L47
Krimigis, S. M., Roelof, E. C., Decker, R. B., & Hill, M. E. 2011, Natur, 474, 359
Kurth, W. S., & Gurnett, D. A. 2020, ApJL, 900, L1
Lindsay, B. G., & Stebbings, R. F. 2005, JGR, 110, A12213
McComas, D. J., Alimaganbetov, M., Beesley, L. J., et al. 2024, ApJS, 270, 17
McComas, D. J., Allegrini, F., Bagenal, F., et al. 2008, SSRv, 140, 261
McComas, D. J., Allegrini, F., Bochsler, P., et al. 2009a, SSRv, 146, 11
McComas, D. J., Allegrini, F., Bochsler, P., et al. 2009b, Sci, 326, 959
McComas, D. J., Shrestha, B. L., Livadiotis, G., et al. 2025, ApJ, 980, 154
McComas, D. J., Shrestha, B. L., Swaczyna, P., et al. 2022, ApJ, 934, 147
McComas, D. J., Swaczyna, P., Szalay, J. R., et al. 2021, ApJS, 254, 19
Mostafavi, P., Adhikari, L., Shrestha, B. L., et al. 2025, ApJ, 979, 222
Reisenfeld, D. B., Bzowski, M., Funsten, H. O., et al. 2021, ApJS, 254, 40
Richardson, J. D., Belcher, J. W., Garcia-Galindo, P., & Burlaga, L. F. 2019, NatAs, 3, 1019
Richardson, J. D., Cummings, A. C., Burlaga, L. F., et al. 2021, ApJL, 919, L28
Richardson, J. D., Kasper, J. C., Wang, C., et al. 2008, Natur, 454, 63
Shrestha, B. L., Zirnstein, E. J., & Heerikhuisen, J. 2020, ApJ, 894, 102
Swaczyna, P., McComas, D. J., Zirnstein, E. J., et al. 2020, ApJ, 903, 48
Zirnstein, E. J., Heerikhuisen, J., Zank, G. P., et al. 2014, ApJ, 783, 129
Zirnstein, E. J., Kim, T. K., Dayeh, M. A., et al. 2022, ApJL, 937, L38
Zirnstein, E. J., McComas, D. J., Kumar, R., et al. 2018, PhRvL, 121, 075102